Available online at www.sciencedirect.com
ScienceDirect
Mechanical Systems and Signal Processing 21 (2007) 1927–1935
Mechanical Systems and Signal Processing
www.elsevier.com/locate/jnlabr/ymssp

Simulation of stochastic vibration of maglev track inspection vehicle

Xingchu Liu*, Xiqiang Guan, Jianwu Zhang

Institute of Automotive Engineering, School of Mechanical Engineering, Shanghai Jiao Tong University, Huashan Road, Shanghai 200030, PR China

Received 18 December 2005; received in revised form 18 August 2006; accepted 25 August 2006
Available online 23 October 2006

Abstract

The stochastic vibration of a maglev track inspection vehicle is the main factor that has direct influence on the accuracy of geometrical measurements of the maglev tracks on board whenever the inspection vehicle is operated at a certain speed. Based upon the principle of motions of the specified vehicle, a vibration model of 5 dof for the maglev track inspection vehicle is proposed and a numerical example is made for the analysis of dynamic responses of the vehicle in stochastic excitation of the maglev track. Effects of vibrations of the vehicle on the accuracy of measuring displacement by laser triangle method are examined. Simulation results of lateral, vertical, roll, pitch, and yaw vibrations for the maglev track inspection vehicle equipped with the measuring system of high precision are provided for the design of the similar vehicles.

Keywords: Maglev track; Inspection vehicle; Stochastic vibration; Track excitation; Laser triangle method

1. Introduction

Transrapid Maglev Transportation System of 30 km range in Shanghai has been already in routine operation for a couple of years, which is the first high-speed train line for commercial purpose. With increase of system operation, it becomes more important that geometrical conditions of maglev tracks for the train safety are required to be detected and reported to the operation centre. Therefore, the present research is carried out for assistance of development of an efficient track inspection vehicle for the Maglev Shanghai.

The maglev track inspection vehicle is well manufactured and equipped to detect deviations of characterised geometrical parameters of the maglev track from its normal condition for safe operation of the maglev train. This special vehicle is supported by eight wheels on the maglev track. During the process of measuring geometrical parameters of the maglev tracks by laser displacement sensors, such factors as measuring environment, light source, tracks surface characteristics and inclination [1–3] and measuring platform have considerable influence on the accuracy of measurement, among which vibrations of the measuring platform of the inspection vehicle is recognised as the key factor. Therefore, efficiency and precision of the measurement

*Corresponding author. Tel.: +86 21 62933178; fax: +86 21 62933772.
E-mail address: lxc@sjtu.edu.cn (Xingchu Liu).

0888-3270/$ - see front matter © 2006 Elsevier Ltd. All rights reserved.
doi:10.1016/j.ymssp.2006.08.010

rely on velocity of the vehicle. The higher the vehicle speed is, the more severe the vehicle vibration is. For the purpose of formulation of the vehicle speed-vibration correlation, a 5 dof vibration model of the inspection vehicle is developed. By imposing the stochastic road excitation of the maglev track to the vehicle at the speed of 10 km/h, influence of vibrations of the vehicle on accuracy of the measurement is studied in numerical way. It is demonstrated by the present results that the laser triangle method can be employed with incorporation of the track inspection vehicle to realise the development of track inspection vehicles of higher efficiency at reasonable speed than those seen before.

2. Vibration modelling of the vehicle with the guide system

The inspection vehicle is mainly composed of vehicle body, measuring system, axles and wheels, guiding arms and wheels, and data acquisition and treatment system. Because the pair of structures for mounting a matrix of laser sensing devices is rigidly connected on both sides of the vehicle body, they are supposed to be one whole rigid frame from viewpoint of engineering application. No sooner is the inspection vehicle treated to be the inertia mass as a whole, on the other hand, vehicle and guiding wheel tires are simplified to be taken by a combination of dampers and linear springs [4].

The position of the vehicle in the space is described by the X, Y and Z coordinates perpendicular to each other with the origin O fixed on the centre of gravity of the vehicle. The rigid body of the vehicle is possessed of 6 dof, as shown in Fig. 1, the vibration of the vehicle can be divided into motions along the X, Y and Z coordinates and rotations around the X, Y and Z ones. Since vibrations in the X coordinate have no effect on the measurement, the vibrations in the Y and Z coordinates are considered and then the vibration model 5 dof

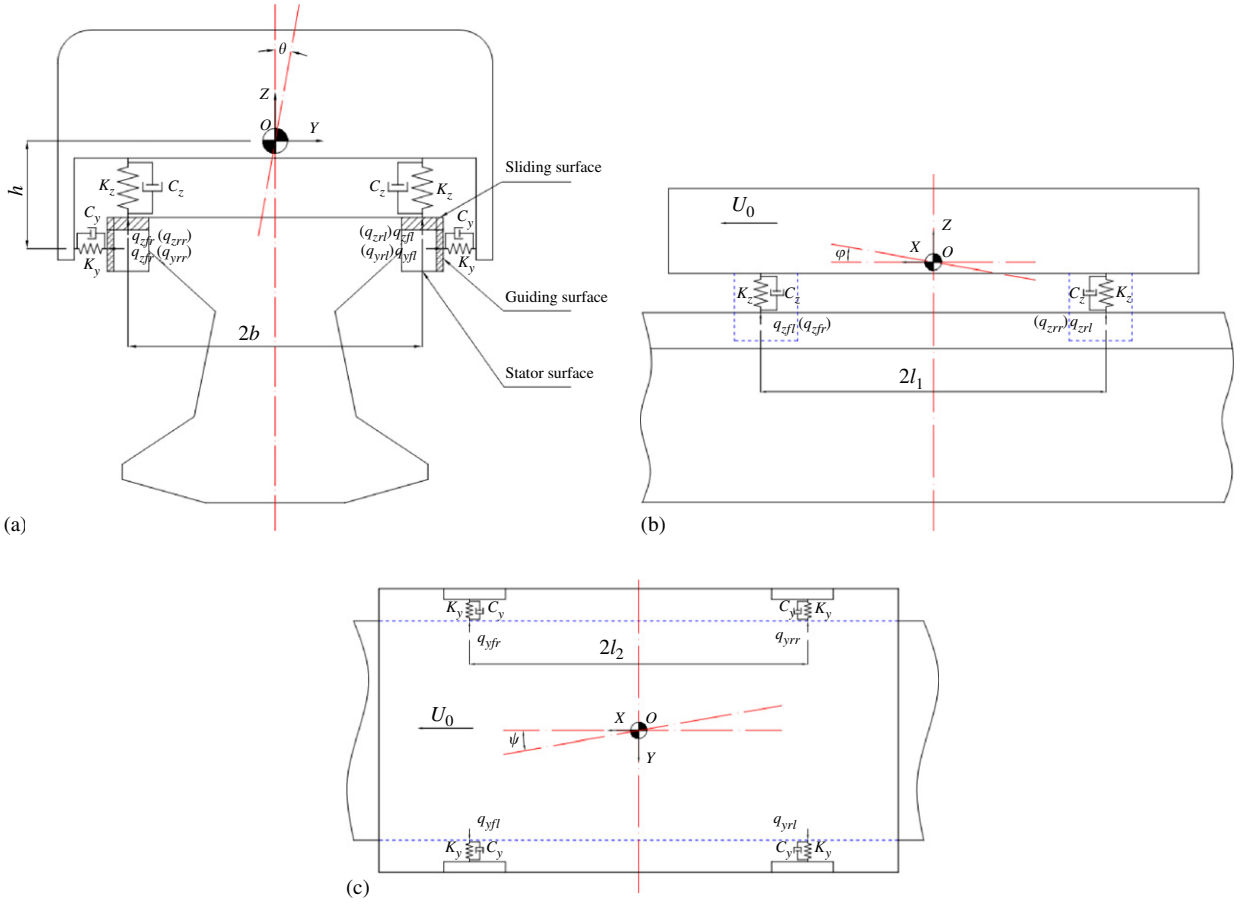

Fig. 1. The vibration model of maglev track inspection vehicle. (a) The front view, (b) the side view and (c) top view.

is proposed, motions of which are, respectively, lateral and vertical displacements, yaw, pitch and roll angles. With consideration of symmetry of the vehicle on the X and Y coordinates, the equilibrium equations governing 5 motions of the vehicle may be expressed in the following:

$$M\ddot{y} + C_y(\dot{y}_{fr} + \dot{q}_{yfr}) + K_y(y_{fr} + q_{yfr}) + C_y(\dot{y}_{rr} + \dot{q}_{yrr}) + K_y(y_{rr} + q_{yrr}) + C_y(\dot{y}_{fl} - \dot{q}_{yfl}) + K_y(y_{fl} - q_{yfl}) + C_y(\dot{y}_{rl} - \dot{q}_{yrl}) + K_y(y_{rl} - q_{yrl}) = 0, \tag{1}$$

$$M\ddot{z} + C_z(\dot{z}_{fr} - \dot{q}_{zfr}) + K_z(z_{fr} - q_{zfr}) + C_z(\dot{z}_{rr} - \dot{q}_{zrr}) + K_z(z_{rr} - q_{zrr}) + C_z(\dot{z}_{fl} - \dot{q}_{zfl}) + K_z(z_{fl} - q_{zfl}) + C_z(\dot{z}_{rl} - \dot{q}_{zrl}) + K_z(z_{rl} - q_{zrl}) = 0, \tag{2}$$

$$I_x\ddot{\theta} - C_y(\dot{y}_{fr} + \dot{q}_{yfr})h - K_y(y_{fr} + q_{yfr})h - C_y(\dot{y}_{rr} + \dot{q}_{yrr})h - K_y(y_{rr} + q_{yrr})h - C_y(\dot{y}_{fl} - \dot{q}_{yfl})h - K_y(y_{fl} - q_{yfl})h - C_y(\dot{y}_{rl} - \dot{q}_{yrl})h - K_y(y_{rl} - q_{yrl})h + C_z(\dot{z}_{fr} - \dot{q}_{zfr})b + K_z(z_{fr} - q_{zfr})b + C_z(\dot{z}_{rr} - \dot{q}_{zrr})b + K_z(z_{rr} - q_{zrr})b - C_z(\dot{z}_{fl} - \dot{q}_{zfl})b - K_z(z_{fl} - q_{zfl})b - C_z(\dot{z}_{rl} - \dot{q}_{zrl})b - K_z(z_{rl} - q_{zrl})b - Mgh\theta = 0, \tag{3}$$

$$I_y\ddot{\varphi} + C_z(\dot{z}_{fr} - \dot{q}_{zfr})l_1 + K_z(z_{fr} - q_{zfr})l_1 - C_z(\dot{z}_{rr} - \dot{q}_{zrr})l_1 - K_z(z_{rr} - q_{zrr})l_1 + C_z(\dot{z}_{fl} - \dot{q}_{zfl})l_1 + K_z(z_{fl} - q_{zfl})l_1 - C_z(\dot{z}_{rl} - \dot{q}_{zrl})l_1 - K_z(z_{rl} - q_{zrl})l_1 = 0, \tag{4}$$

$$I_z\ddot{\psi} + C_y(\dot{y}_{fr} + \dot{q}_{yfr})l_2 + K_y(y_{fr} + q_{yfr})l_2 - C_y(\dot{y}_{rr} + \dot{q}_{yrr})l_2 - K_y(y_{rr} + q_{yrr})l_2 + C_y(\dot{y}_{fl} - \dot{q}_{yfl})l_2 + K_y(y_{fl} - q_{yfl})l_2 - C_y(\dot{y}_{rl} - \dot{q}_{yrl})l_2 - K_y(y_{rl} - q_{yrl})l_2 = 0 \tag{5}$$

and further the relations between the local and general coordinates can be written of the following form:

$$y_{fr} = y - h\theta + l_2\psi, \tag{6}$$

$$y_{rr} = y - h\theta - l_2\psi, \tag{7}$$

$$y_{fl} = y - h\theta + l_2\psi, \tag{8}$$

$$y_{rl} = y - h\theta - l_2\psi, \tag{9}$$

$$z_{fr} = z + b\theta + l_1\varphi, \tag{10}$$

$$z_{rr} = z + b\theta - l_1\varphi, \tag{11}$$

$$z_{fl} = z - b\theta + l_1\varphi, \tag{12}$$

$$z_{rl} = z - b\theta - l_1\varphi, \tag{13}$$

where y_{ij} and z_{ij} $(i = f, r; j = r, l)$ are lateral displacements for guiding wheel tires and vertical displacements for running wheel tires, respectively; M is mass for the vehicle; I_x, I_y and I_z are moments of inertia of the vehicle around the coordinates X, Y and Z, respectively; y is lateral displacement of the vehicle C.G.; z is vertical displacement of the vehicle C.G.; θ, φ and ψ are roll, pitch and yaw angles of the vehicle, respectively; K_y and C_y are stiffness and damping coefficient of the guiding wheel tires, respectively; K_z and C_z are stiffness and damping coefficient of the running wheel tires, respectively; h is the height of the guiding wheel tires to the vehicle C.G.; $2b$ is the running wheel tread symmetric to the vehicle C.G.; $2l_1$ is the running wheel base symmetric to the vehicle C.G.; $2l_2$ is the guiding wheel base symmetric to the vehicle C.G.; g is the acceleration of gravity; q_{ijk} $(i = y, z; j = f, r; k = r, l)$ are unevenness inputs of guiding and sliding surfaces of the maglev track.

3. Stochastic excitation modelling in time domain from maglev track unevenness

The maglev tracks are fixed continuously to overhead concrete girders. Thus, the stochastic characteristics of the track surface unevenness are identical with those of roads of higher grades like aerodrome and expressways. There has been lack of test data of the maglev track surface unevenness by far. Nevertheless, the road unevenness properties of aerodrome can be employed to act as the substitute for the maglev track [5]. This stochastic model in which the white-noise filtration is treated as the input of the vehicle dynamic system in time domain may be expressed in the following form [6]:

$$\dot{q}(t) = -2\pi f_0 q(t) + 2\pi\sqrt{G_0 U_0}\, w(t), \tag{14}$$

where $q(t)$ is the excitation displacement from road unevenness; $\dot{q}(t)$ is the derivative of $q(t)$; f_0 is lower cut-off frequency, commonly 0.1 Hz; G_0 is the road unevenness coefficient related to the road grade and is $1.5 \times 10^{-6}\,\mathrm{m}^3/c$ here; U_0 is vehicle velocity; $w(t)$ is Gauss white noise with zero mean value and 1 variance. Imposition Laplace transform to Eq. (14) results in the input function in frequency domain of the following form:

$$q(s) = \frac{2\pi\sqrt{G_0 U_0}}{s + 2\pi f_0} w(s), \tag{15}$$

where s is the Laplace operator. In Fig. 2, it is shown that the time sequence samples of the track surface unevenness generated from the model are the same as those in Ref. [5] basically, by which the stochastic approximation is validated and parametric values of the track model may be employed in the simulation.

The surface statistic characteristics of the left and right side of maglev track are considered same, so their stochastic track excitation can be generated, respectively. On one side of the maglev track, there exists a time delay function $q_r(t) = q_f(t-\Delta)$ [7] between the track excitation for front tire $q_f(t)$ and the track excitation for rear tire $q_r(t)$, the time delay is $\Delta = l/U_0$, l is the distance from front tire to rear tire. Say, the time function $q_f(t)$ has Laplace transform $q_f(s)$; then, the time delay function $q_r(t) = q_f(t-\Delta)$ has Laplace transform:

$$\frac{q_r(s)}{q_f(s)} = \mathrm{e}^{-\Delta s} \approx \frac{1 - \Delta(s/2)}{1 + \Delta(s/2)}. \tag{16}$$

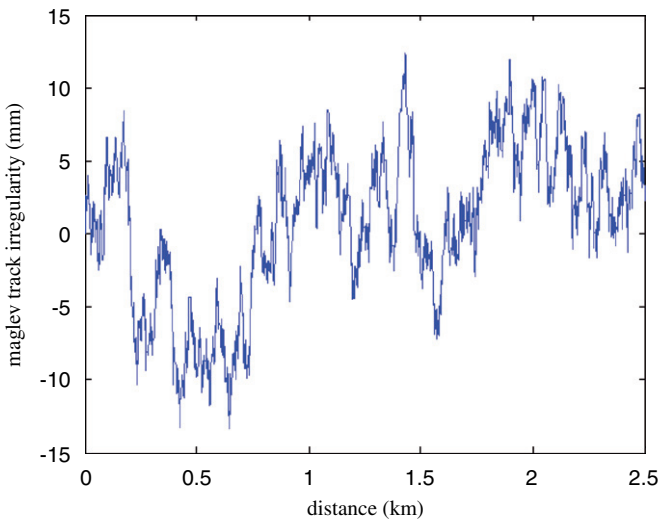

Fig. 2. Time sequence sample of maglev track surface unevenness at the speed of 400 km/h.

Making inverse Laplace transform of Eq. (16) and rearranging the result, we obtain

$$\dot{q}_r(t) = -\frac{2}{\Delta} q_r(t) + \frac{2}{\Delta} q_f(t) - \dot{q}_f(t). \tag{17}$$

4. Simulation and analysis

According to the stochastic excitation model the inputs of maglev track unevenness for both sides of the wheel tracks of the vehicle are generated, respectively. A numerical example is made to show some simulation results of the present research that the vehicle is trailed on the tracks at the fixed $U_0 = 10\,\text{km/h}$ (2.78 m/s) and is characterised by the vibration system parameters as given for details in Table 1. For an arbitrary measuring point $p(x_0, y_0, z_0)$ on board, the displacements in the Y and Z coordinates of the linear vibration system can be rewritten as follows:

$$y_p = y + z_0\theta + x_0\psi, \tag{18}$$

$$z_p = z - y_0\theta + x_0\varphi. \tag{19}$$

Thus, for the measuring point $m(4, 1, -1)$ that is the farthest one from the vehicle C.G. substitution of the coordinates corresponding to point m to Eqs. (18) and (19) yields the following approximations as

$$y_m = y - 1000\theta + 4000\psi, \tag{20}$$

$$z_m = z - 1000\theta + 4000\varphi. \tag{21}$$

Accordingly, simulation results are shown that, respectively, in Fig. 3 for the vibration responses of the measuring point m, in Fig. 4 for the roll angle responses of the vehicle, in Fig. 5 for the pitch angle responses of

Table 1
Physical and geometrical parameters of the vibration system

Parameter	I_x	I_y	I_z	K_y	K_z	C_y
Value	9.22×10^3	28.78×10^3	30.57×10^3	300×10^3	640×10^3	0.8×10^3
Unit	kg m^2	kg m^2	kg m^2	N/m	N/m	N/(m/s)
Parameter	C_z	M	H	b	l_1	l_2
Value	3×10^3	6.6×10^3	0.74	1.1	2.03	2.03
Unit	N/(m/s)	kg	m	m	m	m

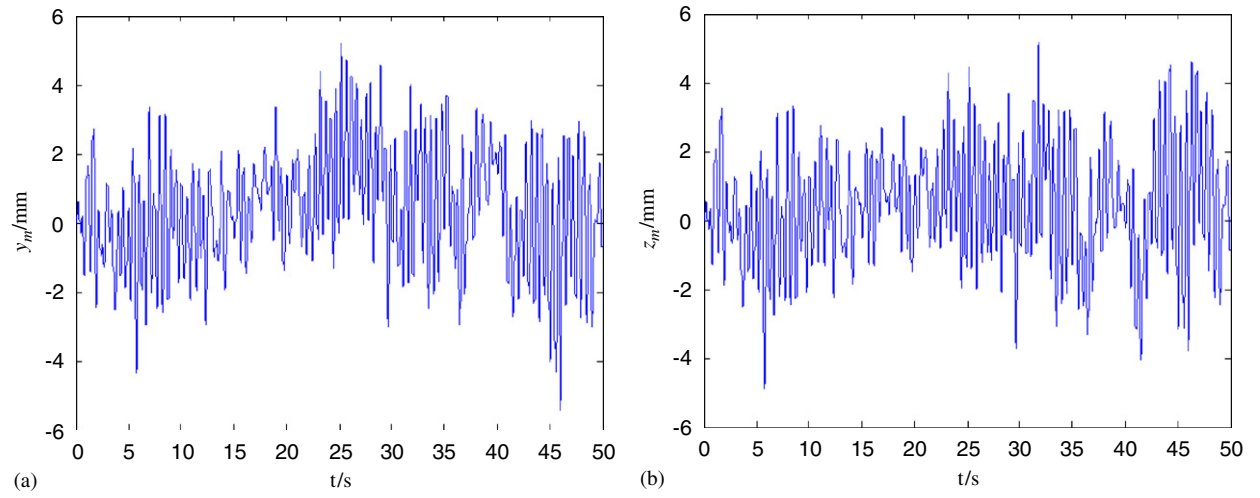

Fig. 3. Numerical results of vibration responses of the measuring point m. (a) Lateral displacement responses and (b) vertical displacement responses.

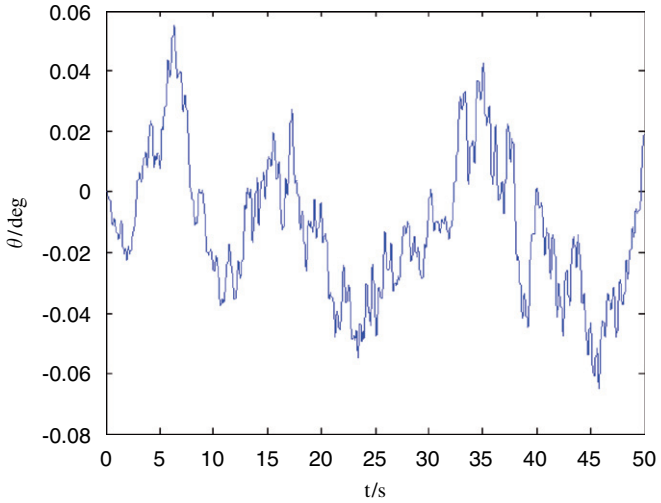

Fig. 4. Numerical results of roll angle responses of the vehicle.

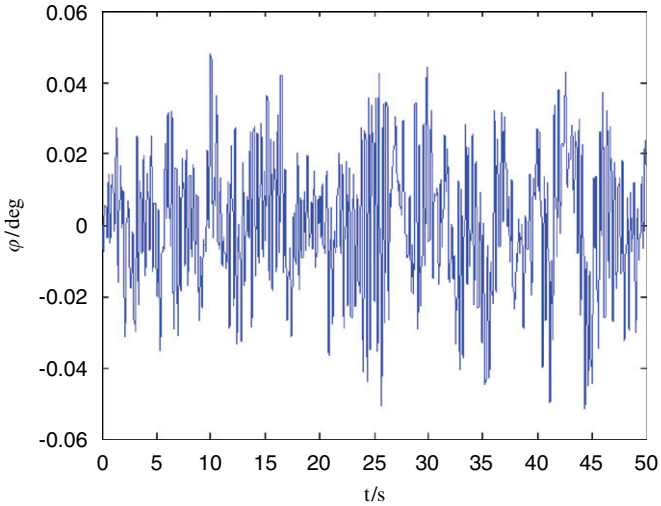

Fig. 5. Numerical results of Pitch angle responses of the vehicle.

the vehicle, and in Fig. 6 for the yaw angle responses of the vehicle. As observed in Figs. 3(a) and (b), the amplitude of transient responses for vertical displacement of the vehicle is almost similar with those for lateral displacement approximately in a range of irregularities from -6 to $+6$ mm. The two vibrations of the vehicle in both vertical and lateral directions are restrained to a reasonable limit by the present chassis vibration isolation system for the inspection vehicle.

After calibration the laser displacement sensors based on triangulation are used to measure relative displacements to the sensing points on the surfaces of the maglev track. Simultaneously, the time series of information of measurement can be processed by the specific signal treatment to determine indexed deviations from the maglev track geometrical parameters such as its width, the distance from sliding surface to stator surface, and so on. Only relative displacements including the vibration are measured. Thus, vibration frequencies are independent of the measurement procedure. The key concerns that affect the measurement accuracy are the limitation of measurement of the laser displacement sensors and the range of angle changes of the vehicle attitude. In Fig. 3 are shown displacement values of vibration responses of the measuring point m,

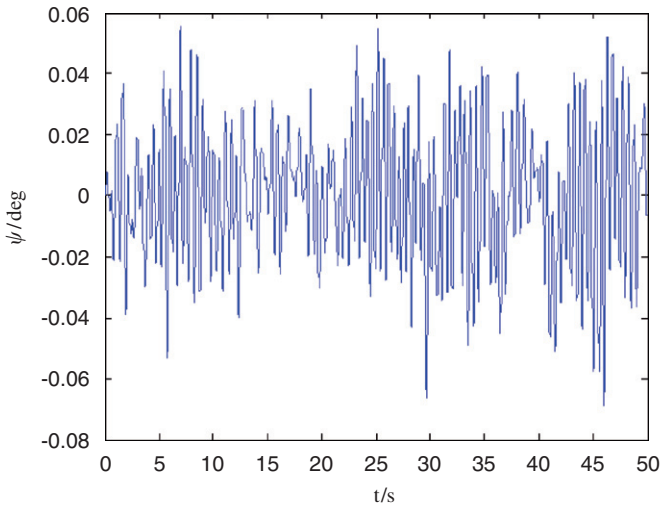

Fig. 6. Numerical results of yaw angle responses of the vehicle.

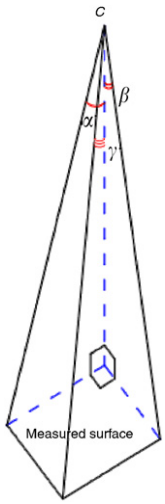

Fig. 7. Sketch map of the attitude of measuring point.

being in all the time less than 6 mm. This means that the real range is within the limitation of laser displacement sensors [8]. As a result, the error of measurement is less than 0.01 mm.

According to the dynamic model of the vehicle, such vibration modes as rotations about the X, Y and Z coordinates exist. Much computational effort has been made to show that influences of the pair of rotations θ and φ on the measurement along the Z coordinate and of the pair of rotations θ and ψ on the measurement along the Y coordinate are considerable. As shown in Fig. 7, the measuring point c is the position of any one of the laser displacement sensors perpendicular to the measured surface when the vehicle is in static state. In the case of on-board measuring dynamically, the three angles obey the spatial geometrical relation of the following form as $tg\gamma = \sqrt{tg^2\alpha + tg^2\beta}$. We can obtain $\gamma \leqslant \alpha + \beta$ when $0 \leqslant \alpha, \beta < \pi/4$. Because $|\theta|$, $|\varphi|$ and $|\psi|$ are less than 0.08°, respectively, as shown in Figs. 4–6, the angle of attitude of the measuring point c is less than 0.16° and then the error caused in measurement is evaluated to be 0.025 mm [9]. It is concluded, therefore, that the measuring error induced due to the vehicle vibration is much less in comparison with the required of measurement for the measuring system when the inspection vehicle is operated at the speed of 10 km/h (2.78 m/s).

According to Eqs. (18) and (19), if there are two arbitrary measuring points p'_1 and p'_2 from which the values of the coordinate Z are identical and can be determined in the following form:

$$\psi = \frac{y_{p'_1} - y_{p'_2}}{l_{p'}}, \tag{22}$$

where $y_{p'_1}$ and $y_{p''_1}$ are, respectively, displacements of the measuring points p'_1 and p'_2 along the coordinate Y in the same time, $l_{p'_1}$ is the distance from p'_1 to p'_2 in the coordinate X. If there are two arbitrary measuring points p''_2 and p''_2 from which the values of the coordinate Y are the same and can be determined in the following form:

$$\varphi = \frac{z_{p''_1} - z_{p''_2}}{l_{p''}}, \tag{23}$$

where $z_{p''_1}$ and $z_{p''_2}$ are, respectively, displacements of the measuring points p''_1 and p''_2 along the coordinate Z at the same time, $l_{p''}$ is the distance from p''_1 to p''_2 in the coordinate X. If there are two arbitrary measuring points p'''_1 and p'''_2, from which values of the coordinate X are the same and can be determined in the following form:

$$\theta = \frac{z_{p'''_1} - z_{p'''_2}}{l_{p'''}}, \tag{24}$$

where $z_{p'''_1}$ and $z_{p'''_2}$ are, respectively, displacements of the measuring points p'''_1 and p'''_2 along the coordinate Z in the same time, l_p is the distance from p'''_2 to p'''_1 in the coordinate Y.

Consequently, ψ, φ and θ can be calculated by Eqs. (22)–(24) based on the measuring values of the sensors, which can provide error compensation for the maglev track geometry parameters measuring.

5. Concluding remarks

The vibration model of 5 dof of the maglev track inspection vehicle is developed for numerical analysis of stochastic correspondence of the vehicle speed to the accuracy of the laser triangular measurement. For the simulation of random vibrations of the inspection vehicle the input of the vehicle dynamic system is also modelled for the track surface unevenness with higher-grade road stochastic properties. The stochastic excitation for the maglev track irregularities is characterised with the same range of amplitude and the identical statistic properties. Multiple samples are simulated and the results are same basically.

The present vibration model is applied for real-time dynamic simulation of the correlation between the accuracy of measurement and the velocity of the inspection vehicle and then provided with a matrix of laser displacement sensors for the development of more efficient track inspection vehicle carrying on board the measuring system.

Acknowledgements

The authors would like to express grateful appreciation to China Ministry of Science and Technology and National Maglev Transportation Research and Development Center for the financial support from the State High-Technology Development Program (863) Special Project High-Speed Maglev Transportation System under Grant No. 2001AA505000-114.

References

[1] M.-C. Amann, T. Bosch, M. Lescure, et al., Laser ranging: a critical review of usual techniques for distance measurement, Optical Engineering 41 (1) (2001) 10–19.

[2] K.-C. Kim, S.B. Oh, S.H. Kim, et al., Design of a signal processing algorithm for error-minimized optical triangulation displacement sensors, Measurement Science and Technology 12 (2001) 1683–1688.

[3] W. Jian-feng, W. Wen, C. Zi-Chen, Study on the analysis for error in triangular laser measurement and the method improving accuracy, Mechanical & Electrical Engineering Magazine 20 (5) (2003) 89–91 (in Chinese).

[4] Z. Yu, Automobile Theory, Mechanical Industry Press, Beijing, China, 2002 (in Chinese).

[5] Z. Chunfa, Z. Wanming, W. Kaiyun, A study on maglev vehicle vertical random vibration and ride quality, China Mechanical Engineering 13 (16) (2002) 1402–1407 (in Chinese).

[6] Y. Fan, G. Konghui, Adaptive and self-tuning control of vehicle suspensions, Automotive Engineering 20 (4) (1998) 193–200 (in Chinese).
[7] Z. Yonglin, Z. Jiafan, Numerical simulation of stochastic road process using white noise filtration, Mechanical Systems and Signal Processing 20 (2) (2006) 363–372.
[8] F. Jun-yan, F. Qi-bo, K. Cui-fang, Present status of high precision laser displacement sensor based on triangulation, Applied Optics 25 (3) (2004) 33–36 (in Chinese).
[9] H.-Y. Feng, Y. Liu, F. Xi, Analysis of digitizing errors of a laser scanning system, Precision Engineering 25 (2001) 185–191.